JOURNAL OF MAGNETIC RESONANCE **128,** 70–81 (1997)
ARTICLE NO. MN971212

Rotational Correlation Times of Internuclear Vectors in a DNA Duplex with G–A Mismatch Determined in Aqueous Solution by Complete Relaxation Matrix Analysis of Off-Resonance ROESY (O-ROESY) Spectra

Kazuo Kuwata,*[,1] He Liu,† Thomas Schleich,* and Thomas L. James†

*Department of Chemistry and Biochemistry, Sinsheimer Laboratories, University of California, Santa Cruz, Santa Cruz, California 95064; and †Department of Pharmaceutical Chemistry, University of California, San Francisco, San Francisco, California 94143-0446

Received February 17, 1997; accepted June 30, 1997

Complete relaxation matrix analysis of the off-resonance ROESY (O-ROESY) spectra is presented and demonstrated for a synthetic DNA duplex with two G–A mismatches, *d*(GCTGTC-GAAAGC)$_2$, in solution. The internuclear distance and the rotational correlation time of the internuclear vector could be garnered simultaneously using complete relaxation matrix analysis of O-ROESY, by which spin diffusion effects could be accommodated. Correlation times in the terminal and the mismatched regions were significantly reduced compared to those in other regions, indicating the conformational flexibility of the mismatched pair. The average structure obtained by restrained molecular dynamics simulation with inclusion of variations of the rotational correlation times also indicated a general tendency of the mismatched and contiguous bases to flip to the outside of the double strand. Off-resonance ROESY combined with the complete relaxation matrix analysis method may offer an alternative way to investigate the structures and dynamics of biological macromolecules. © 1997 Academic Press

The three-dimensional structure of any molecule can be determined with a sufficient number of experimental structural constraints, e.g., internuclear distances and bond torsion angles, in conjunction with the holonomic constraints of bond lengths, bond angles, and atom connectivities. To date, every protein or nucleic acid solution structure determined by way of multidimensional NMR experiments has utilized the interproton distance constraints embodied in the cross-peak intensities of nuclear Overhauser effect spectra or rotating frame Overhauser effect spectra. However, the intensity of a particular cross-peak depends not only upon the distance between the two protons corresponding to the cross-peak, but also upon the surrounding proton environment and upon molecular motions. The surrounding protons lead to multispin effects, often termed ''spin-diffusion,'' but these can be accommodated using a complete relaxation matrix analysis of cross-peak intensities (*1, 2*). A correlation time characterizing molecular motions is generally estimated independently of the NOESY or ROESY spectra using one of several methods and may be utilized when analyzing the intensities to obtain distances.

Recently, it has been reported that the information on internuclear distances and on correlation times can be separated using the off-resonance ROESY pulse sequence by eliminating the zero quantum transition effect due to Hartmann–Hahn transfer (*3–5*). This report presents a novel formulation of the off-resonance ROESY (O-ROESY) method (*3, 4, 6*) and its application to a DNA duplex with complete relaxation matrix analysis to overcome several difficulties associated with the original O-ROESY cross-peak intensity analysis (*6*). Furthermore, we demonstrate that this approach can enable the garnering of both distance constraints and motional information from the O-ROESY spectra by encoding the spectrum along the off-resonance spin-lock frequency axis rather than the mixing time axis.

COMPLETE RELAXATION MATRIX ANALYSIS PROGRAMS FOR O-ROESY

The cross-relaxation rate in the O-ROESY experiment $\sigma_{\text{O-ROE}}$ can be expressed as (*3, 4*)

$$\sigma_{\text{O-ROE}} = \frac{1}{10}\left(\frac{h}{2\pi}\right)^2 \frac{\gamma^4}{r_{kl}^6} \times \left\{\frac{|(\omega_k - \omega_{\text{RF}})(\omega_l - \omega_{\text{RF}})|\,\sigma_{\text{NOE}} + \omega_2^2\sigma_{\text{ROE}}}{\Omega_k\Omega_l}\right\}, \quad [1]$$

[1] Present Address: Department of Physiology, School of Medicine, Gifu University, Gifu 500 Japan. Fax: +81(58)-267-2962. E-mail: kuwata@cc.gifu-u.ac.jp.

1090-7807/97 $25.00

where ω_i is the Larmor precession frequency of spin i ($i = k$, l); ω_{RF} is the maximum excitation frequency of off-resonance spin-lock pulse; ω_2 is γB_2; B_2 is the field strength; $\Omega_i = \{(\omega_i - \omega_{RF})^2 + \omega_2^2\}^{1/2}$ ($i = k$, l); r_{kl} is the internuclear distance between the k- and l spins; $\sigma_{NOE} = -J(0) + 6J(2\omega)$; $\sigma_{ROE} = 2J(0) + 3J(\omega)$; and γ is the gyromagnetic ratio. Although a Lipari–Szabo-type spectral density function including anisotropic overall tumbling motions (*7*) is fully implemented in the proposed programs, more than two different static magnetic fields are required to obtain relevant parameters in the spectral density function (cf. Appendix II). Also its applicability to the nonbonded internuclear vectors is still ambiguous. Thus for the purpose of this report, it is enough to use a single static magnetic field and a simplified spectral density function for the isotropic rotational motion

$$J(n\omega) = \frac{\tau_{kl}}{1 + n^2\tau_{kl}^2\omega^2}, \qquad [2]$$

where τ_{kl} is the generalized correlation time of specific internuclear vector. Using nonlinear curve fit of $\sigma_{O\text{-}ROE}$ values, which are obtained using the complete relaxation matrix analysis of O-ROESY as described below, we can obtain r_{kl} and τ_{kl} independently.

Cross-peak intensities can be converted into cross-relaxation rate constants using the complete relaxation matrix analysis, e.g., MARDIGRAS program (*1*), which supplements the observed intensities with calculated values from the model structure in order to avoid the singularity in the matrix computations. We coded three programs for the complete relaxation matrix analysis for the O-ROESY experiment, i.e., CORMA-O-ROESY, MARDIGRAS-O-ROESY, and NONLINEAR-O-ROESY. For CORMA-O-ROESY and MARDIGRAS-O-ROESY, we modified CORMA and MARDIGRAS programs, respectively (*1*); that is, we replaced the self-relaxation equations of equivalent protons and cross-relaxation equations of all the protons for on-resonance ROESY experiment with those for off-resonance ROESY (O-ROESY) according to Ref. (*4*). In addition, for MARDIGRAS-O-ROESY, we modified the interface to include the variations of τ_{kl} values which are externally given by NONLINEAR-O-ROESY program. Using MARDIGRAS-O-ROESY, cross-relaxation rates $\sigma_{O\text{-}ROE}$ can be calculated simultaneously for all the cross-peak intensities of an O-ROESY spectrum with spin-diffusion taken into account. Application of MARDIGRAS-O-ROESY to a series of O-ROESY spectra results in a nonlinear dispersion curve $\sigma_{O\text{-}ROE}$ as a function of ν_{irrad}, which is a frequency difference between the center of the chemical shift of two spins and the excitation maximum frequency of the composite pulse. NONLINEAR-O-ROESY is for the nonlinear curve fit of the theoretical cross-relaxation rate dispersion curve to the experimental cross-relaxation rates in order to obtain both r_{kl} and τ_{kl}.

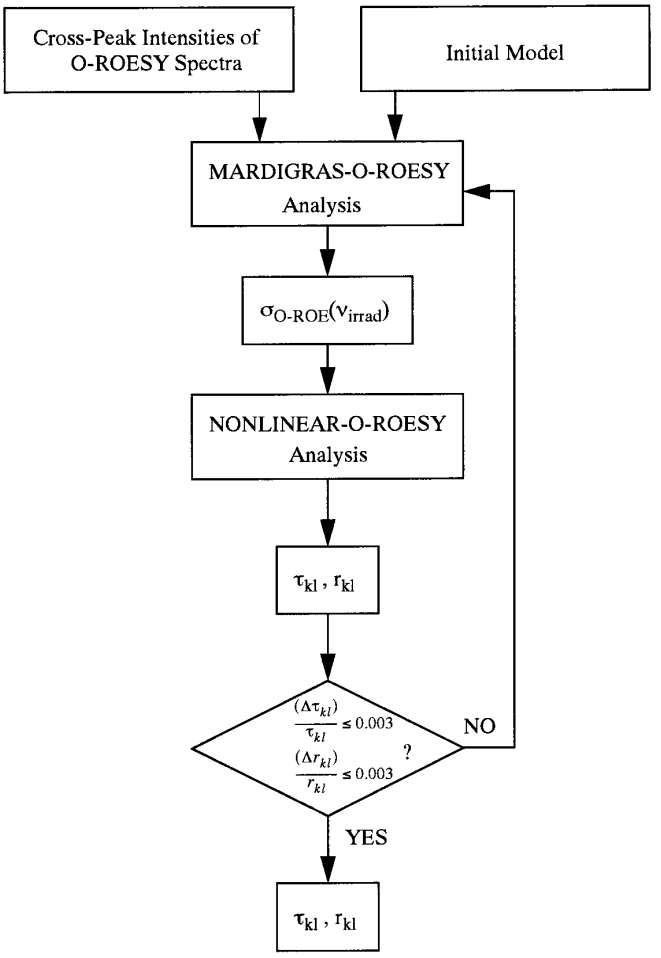

FIG. 1. Flow diagrams of the complete relaxation matrix analysis of the O-ROESY spectra. Cross-peak intensities of O-ROESY spectra are analyzed using MARDIGRAS-O-ROESY to yield the cross-relaxation rates ($\sigma_{O\text{-}ROE}$) as a function of ν_{irrad}, which are subsequently used for the nonlinear curve fit using NONLINEAR-O-ROESY to yield both r_{kl} and τ_{kl} values. To achieve the correct normalization factor, above procedures are repeated several times (see text).

As shown in Fig. 1, we employed the following procedure: (1) MARDIGRAS-O-ROESY calculation on the O-ROESY spectra to obtain $\sigma_{O\text{-}ROE}$ as a function of ν_{irrad}. (2) Nonlinear curve fitting of $\sigma_{O\text{-}ROE}$ to yield the unique set of r_{kl} and τ_{kl} simultaneously, using NONLINEAR-O-ROESY. The parameters r_{kl} and τ_{kl} were refined with iterative loops that use r_{kl} and τ_{kl} resulting from the previous curve fitting as the input for calculation of new cross-relaxation rates in the next curve fitting step; thereby we could obtain the correct normalization factor between the calculated intensities and the experimental intensities. Of course, we can use the optimized τ_{kl} values for the MARDIGRAS calculation on NOESY spectra. These three programs are available via e-mail to james@picasso.ucsf.edu, yoti@aku.ucsc.edu, or kuwata@cc.gifu-u.ac.jp.

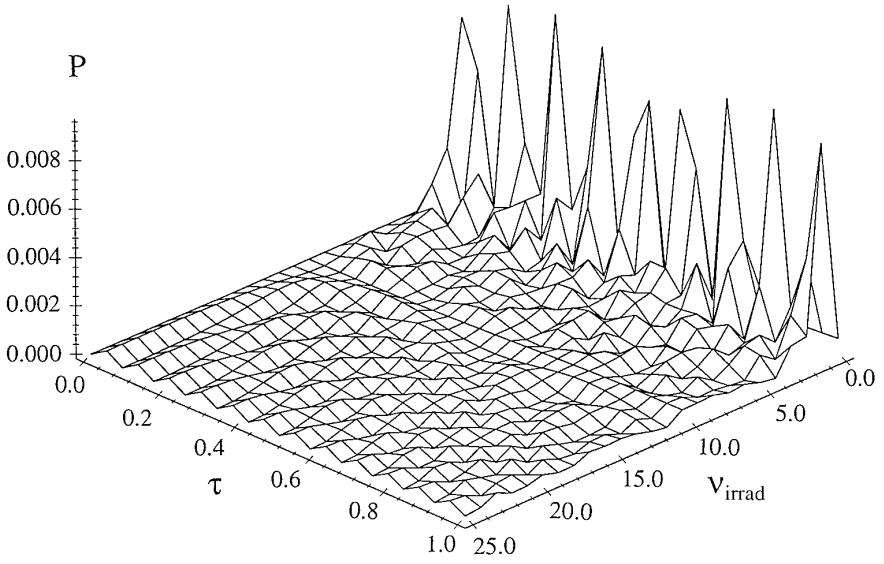

FIG. 2. ZQT probability P_{kl} for a coupled pair of k and l spins (J = 5 Hz, $\omega_k = -\omega_l = 2\pi \times 250$ Hz) under the off-resonance irradiation field ($\omega_2 = 2\pi \times 5000$ Hz) as a function of off-resonance irradiation frequency ν_{irrad} (kHz) = $\omega_{\text{RF}}/(2\pi \times 10^3)$ and mixing time τ (s).

MATERIALS AND METHODS

Materials

The oligonucleotide, GCTGTCGAAAGC, was made on a Cyclone Plus Milligen/Bioresearch DNA synthesizer using a 15-μmol phosphoramidite column. The oligonucleotide was synthesized with the final DMT group left on the molecule, and was removed from the column by treatment overnight with 30% ammonium hydroxide and then lyophilized to dryness. It was resuspended in TEAA buffer and purified using a 625 HPLC (Waters) with a C18 column (Bondapak) and run over a gradient of 95% TEAA/5% acetonitrile to 65%/35% over 30 min. The fraction containing the oligonucleotide was lyophilized and treated for 20 min with 80% acetic acid to remove the DMT group. The acetic acid was lyophilized off and the DNA was resuspended in TEAA for a second run on the HPLC with a gradient of 80/20 TEAA/acetonitrile to 65/35 for 60 min. The main peak was collected and lyophilized. The sample was redissolved in nanopure water and loaded onto a 3g Sep-Pac column and washed with 10 ml of nanopure water to remove buffer salts. The oligonucleotide was eluted with 6 ml of 40% acetonitrile/water and then lyophilized again. The last purification step consisted of eluting the oligonucleotide through a C-25 CM-Sephadex column which had been equilibrated with 1.0 *M* NaCl. The elute was collected and lyophilized. Approximately 2 mmoles of DNA were dissolved in 0.5 ml of 20 m*M* phosphate buffer (pH 7.5). NMR spectra were recorded in either 99.99% D_2O or 90% H_2O/10% D_2O.

NMR Experiments

Phase sensitive O-ROESY experiments were conducted on a Varian Unityplus 500-MHz NMR spectrometer equipped with a programmable pulse modulator and a 5-mm Varian pulse field gradient triple resonance probe. Data were acquired using the hypercomplexed method of phase cycling with a spectral width of 5950 Hz. Typically, 2048 t_2 points (1024 real) and 256 (real) t_1 increments were collected. Spectra were zero-filled in the t_1 dimension to 2048 (1024 real) points prior to Gaussian function weighting in both dimensions and Fourier transformation. The digital resolution was 5.8 Hz in both dimensions. A 60-ms mixing time was empirically determined to represent the optimal values. A recycle delay of 2 s was used.

A frequency-shifted laminar pulse (SLP) (*8*) was used to maintain phase coherence between the off-resonance spin-lock pulse and the hard $\pi/2$ pulse as described previously (*3*). Shifted laminar pulse, 60 ms in duration, at the desired frequencies were composed of 60,000 ''laminates'' of a prescribed phase and constant amplitude, each of 1 μs duration. The field strength of the spin-lock pulse used was 5.1 kHz (1.2 G). The off-resonance spin-locking frequency was varied from 0 to 20 kHz. Phase sensitive NOESY experiments were performed at mixing times of 100, 200, and 300 ms. All the experiments were performed at 25°C. NMR data reduction, assignments, and volume integration were performed using the Striker and Sparky 2.0 software (UCSF).

Dressed State Representation of the ZQT Probability in the Off-Resonance Irradiation Field

Although the ratio of cross-relaxation rates of NOESY (σ_{NOE}) to ROESY (σ_{ROE}) was utilized for the investigation of macromolecular hydration dynamics (*9*), it was difficult to quantify σ_{ROE} of the intramolecular internuclear vector because of the J-coupled zero-quantum transition (ZQT)

(*10*). Recently it was reported that the Hartmann–Hahn transfer can be eliminated in the off-resonance irradiation field in case of continuous wave irradiation (*5*). Here, we first formulate the effect of *J*-coupled ZQT to the O-ROESY spectra using a dressed state representation in a superimposed tilted doubly rotating frame (STDRF) (*11*) based on quantum electrodynamical (QED) theory (*12*) in order to avoid several limitations associated with the average Hamiltonian theory on the composite (shaped) pulses (*13*). This novel formulation is described in Appendix I. In the case of the shaped pulse with constant phase increment and constant amplitude, we finally obtained the *J*-coupled zero quantum transition probability between the *k* and *l* spins, $P_{kl}(\tau)$

$$P_{kl}(\tau) = |U_{kl}(\tau)|^2 = \frac{\Omega_R^2}{\Omega^2} \sin^2\left(\frac{\Omega\tau}{2}\right), \qquad [3]$$

where U_{kl} is the transition amplitude; Ω_R is the generalized Rabi frequency defined in Eq. [5] in Appendix I; $\Omega = \Omega_R^2 + \Delta^2$; Δ is the difference of effective precession frequency between the *k* and *l* spins; and τ is the mixing time. P_{kl} rapidly decreases in an oscillatory manner as the off-resonance irradiation frequency (ν_{irrad}) increases as shown in Fig. 2. This calculation was performed on a Sparc 20 computer using the program Maple V (Release 3, 1994, Waterloo Maple Software). Around the tilt angle, which is the angle between the *z* axis and the quantization axis, $\sim(\pi/2 -$ magic angle), i.e., $\nu_{irrad} \sim 7.1$ kHz, P_{kl} becomes smaller than 0.001, which almost corresponds to the results of Desvaux *et al.* (*5*). Although for the AX_n system ($n > 1$), we must diagonalize multiple (>2) energy levels, the behavior of P_{kl} does not change much, and the above conclusion remains valid. In conclusion, we can obtain r_{kl} and τ_{kl} independently and also eliminate *J*-coupled ZQT contribution by use of the complete relaxation matrix analysis of O-ROESY.

Generation of Three-Dimensional Structures

For the structure calculation, restrained molecular dynamics (rMD) was conducted using NMRchitect software (BIOSYM INC.). While proton coupling constant values for deoxyribose were obtained by simulating DQF-COSY cross-peaks with the programs SPHINX and LINSHA (*14, 15*), structures of the DNA duplex were obtained solely on the basis of distance constraints in the rMD procedure. We prepared two kinds of initial conformations for the G–A pair, that is, G_{anti}–A_{anti} and G_{anti}–A_{syn}, as starting structures for restrained molecular dynamics. We note, however, that the cross-peak intensity of *A*9H8–*A*9H1′ in NOESY spectra at short mixing time was extremely weak compared to those of H5–H6 of C2, C6, or C12, strongly suggesting G_{anti}–A_{anti} was the dominant structural characteristic (*16*). Therefore for rMD calculations to assess characteristics of the average structure, we used G_{anti}–A_{anti} conformation as the starting structure.

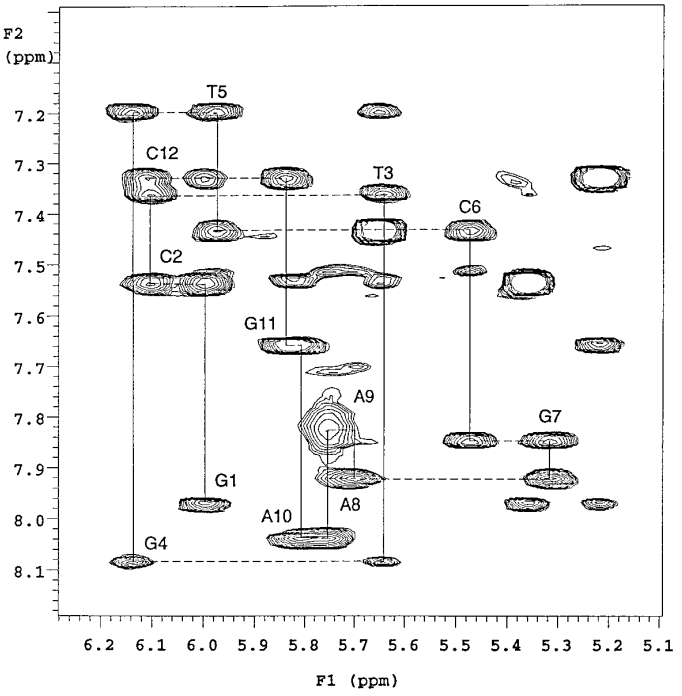

FIG. 3. Sequential assignment of oligonucleotide, *d*(GCTGTCGAAAGC)$_2$, showing the cross-peaks between the sugar H1′ and the base H6/H8 in a NOESY spectrum at a mixing time of 300 ms. Intraresidue cross-peaks at the mismatched residues, i.e., G4 and A9, are small in area and blurred, respectively. The cross-peak between A8H1′ and A9H8 is also hardly observed. The oligonucleotide, GCTGTCGAAAGC, was made on a Cyclone Plus Miligen/Bioresearch DNA synthesizer using a 15-μmol phosphoramidite column. Finally the lyophilized sample was dissolved in 20-m*M* phosphate buffer (pH 7.5) in 99.99% D_2O. All the measurements were conducted at 25°C.

Two distance constraint sets were used: (a) distance constraint set obtained by the MARDIGRAS calculation on NOESY spectra uniformly assuming the same τ_{kl} for all the internuclear vectors, that is, the average value we previously obtained for this size duplex, 2.6 ns at 25°C (*17*); (b) distance constraint set obtained by the complete relaxation matrix analysis for O-ROESY shown in Fig. 1. In addition to the experimentally derived distances, Watson–Crick hydrogen bond restraints based on imino resonances observed in the NOESY spectra in H_2O, that is, base pairs (A10, T3), (G11, C2), (C6, G7) were used. The number of distance constraints used in two different sets were common: 150 intraresidue, 54 interresidue, and 16 hydrogen bond distance constraints.

Restrained molecular dynamics calculations were performed in vacuo using AMBER potential field parameters (*18*). Hydrated Na^+ counterions were added at a distance of 0.5 nm to the phosphorus atoms initially to neutralize the negative charge. The electrostatic term was calculated using a distance-dependent dielectric constant and the cut-off value

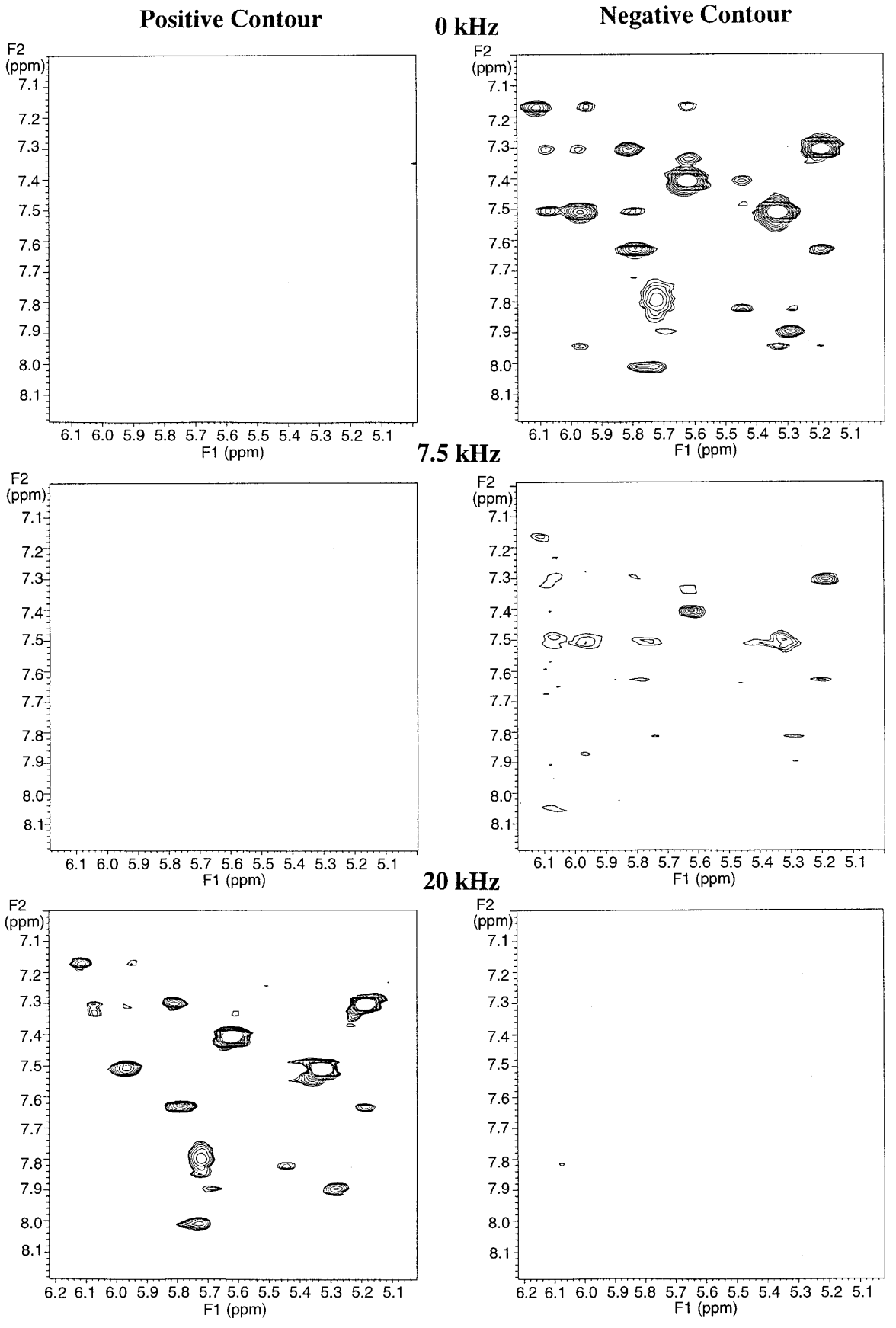
Positive Contour
0 kHz
Negative Contour
7.5 kHz
20 kHz
F2 (ppm)
F1 (ppm)

for nonbonded interactions was 2.0 nm. The annealing protocol was as follows: initial 100 steps, energy minimization using the steepest descent method; 500 steps, energy minimization using the conjugate gradient method; using a 1-fs time step, 5-ps of rMD during which the temperature was raised linearly from 100 to 900 K; rMD at 900 K for 5 ps; and, as the temperature was decreased to 300 K, rMD for 3 ps. A further 12 ps of rMD was then carried out at 300 K, and finally restrained minimization using conjugate gradient method was conducted. Twenty structures were collected by repeating this process and averaged. Average structures were analyzed using Curves 4.1 (*19*).

RESULTS

Proton Resonance Assignments

Nonexchangeable protons were assigned using established techniques for right-handed, double-stranded nucleic acids (*20*, *21*) using DQF-COSY and 2D NOESY. Spin systems in the sugar moiety of the DNA strand could be easily identified in the DQF-COSY spectrum. Sequential assignments in H6/H8−H1′ region are shown in Fig. 3. All the resonances, including all H4′ and most of H5′ and H5″, were assigned. The different intensities of the cross-peaks of H1′ and H2″ at a short mixing time were used to stereospecifically assign H2′ and H2″ resonances in deoxyriboses. Stereospecific assignments of H5′ and H5″ could not be performed without further structural assumptions. Assignment pathways between cross-peaks connecting each base with its own sugar and the 3′ neighbor could be followed in the H6/H8−H1′ and in the H6/H8−H2′/H2″ regions. The intraresidue H8−H1′ cross-peak of G4 was small in area and that of A9 was significantly broadened, indicating the conformational flexibility of the mismatched region. Exchangeable protons could be easily assigned by following well-established strategies (*22*). Imino H3 protons in thymines were identified by their strong interstrand cross-peaks with H2 of the base-paired adenines. Additional cross-peaks to the H2 of the 3′ neighbor were also observed. Amino protons of adenines were assigned by their cross-peaks with H3. Labile protons in GC base pairs were assigned by following their connection to H5 of cytosines (H5C → HN4C → H1G). Except for two terminal residues and two mismatched pairs, all imino protons were identified. No amino proton resonance from guanine was observed.

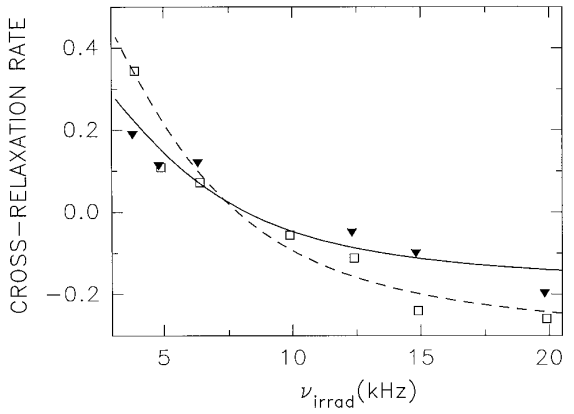

FIG. 5. Cross-relaxation rates vs off-resonance irradiation frequency (ν_{irrad}), which is a frequency difference between the center of the chemical shift of two spins and the excitation maximum of SLP, obtained for proton pairs, A10H2″−G11H8 (▼) and G11H2″−C12H6 (□). Cross-relaxation rates were obtained by the complete relaxation matrix analysis for O-ROESY spectra. The solid lines are the theoretical curves obtained by a fit to the experimental data, and are described by the following parameters for the connectivities A10H2″−G11H8 and G11H2″−C12H6, respectively: internuclear distance, r_{kl}, 2.6 and 2.5 Å; rotational correlation time, τ_{kl}, 1.1 and 1.5 ns (temperature = 25°C).

Nonlinear Curve Fit of the Cross-Relaxation Rates as a Function of the Off-Resonance Spin-Lock Frequency

Figure 4 shows the O-ROESY spectra of the synthetic DNA in the H6/H8-H1′ region at different excitation maximum frequencies of SLP, which are measured from the carrier frequency (4.80 ppm). Clear negative cross-peaks (upper two panels) relative to the positive diagonal peaks are observed in on-resonance ROESY (0-kHz off-resonance spectrum). These cross-peaks almost vanish at 7.5 kHz off-resonance (center two panels). The lower two panels clearly show the positive cross-peaks at 20 kHz off-resonance, indicating a predominantly NOESY character. The field strength of SLP used was 5.1 kHz (1.2 G).

Examples of the nonlinear curve fits using NONLINEAR-O-ROESY are shown in Fig. 5. Cross-relaxation rates calculated by MARDIGRAS-O-ROESY are plotted vs ν_{irrad}. Solid lines indicate the theoretical curves using optimized r_{kl} and τ_{kl} values. We omitted the cross-relaxation rates at $\nu_{irrad} <$ 3 kHz for the nonlinear curve fit to exclude the ZQT effect. [r_{kl} (Å), τ_{kl} (ns)] obtained by NONLINEAR-O-ROESY for two proton pairs A10H2″−G11H8 (▼) and G11H2″−C12H6 (□) were [2.6 ± 0.1, 1.1 ± 0.2] and [2.5 ± 0.1, 1.5 ± 0.2], respectively. Errors were estimated according to Ref. (*23*).

FIG. 4. O-ROESY spectra of the synthetic DNA showing the region of H1′ sugar protons and the aromatic base protons, as a function of the offset of the excitation maximum of SLP measured from the carrier frequency (4.80 ppm). Clear negative cross-peaks (upper two panels) relative to the positive diagonal peaks are observed in on-resonance O-ROESY spectrum (0 kHz off-resonance). These cross-peaks almost vanish at 7.5 kHz off-resonance (center two panels). Lower two panels clearly show the positive cross-peaks at 20 kHz off-resonance, indicating a predominantly NOESY character. The field strength of SLP used was 5.1 kHz (1.2 G).

Values for the correlation time τ_{kl} of the intraresidue and the interresidue interproton vectors are plotted as a function of the residue number (n) in Fig. 6. τ_{kl} values for the interresidue interproton vectors (same strand) between n and $n + 1$ are placed at $n + \frac{1}{2}$. Interresidue interproton vectors between the nth and mth ($m > (n + 1)$) residues, i.e., interstrand interproton vectors, are not included. τ_{kl} values at terminal, mismatched (residues 4 and 9) and contiguous (residues 7 and 8) residues of the DNA molecule seem to be somewhat smaller than those at other residues, suggesting the conformational flexibility. r_{kl} and τ_{kl} values calculated using the complete relaxation matrix analysis of O-ROESY are listed in Table 1.

Average Structures of DNA

Figure 7A shows the structure of synthetic DNA duplex which is an average of 20 structures generated by a simulated annealing procedure using distance constraint set (a) (A-conformation). Figure 7B shows the averaged structure using the distance constraint set (b) obtained by the O-ROESY complete relaxation matrix analysis (B-conformation). Statistics of the superimposition of the converged structures are listed in Table 2. Root mean square deviation (RMSD) between conformations A and B are three times as large as those within each of the 20 structures, indicating that A and B may be different conformations. The relative potential energy of B is smaller than that of A by 74 kcal/mol, indicating that B conformation is energetically more favorable.

Global interbase pair parameters, shear (*Sx* Å), stretch (*Sy* Å), and stagger (*Sz* Å), of two final averaged structures obtained using the Curves 4.1 program (*19*) are plotted vs

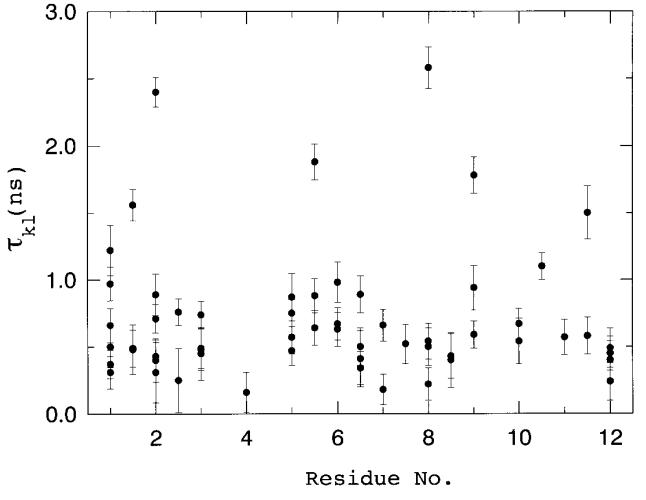

FIG. 6. τ_{kl} values (ns) of the intraresidue and interresidue interproton vectors, as a function of the residue number (n). τ_{kl} values for the interresidue interproton vectors (same strand) between n and $n + 1$ are placed at $n + \frac{1}{2}$. Interstrand interproton vectors are not included.

TABLE 1
Rotational Correlation Times and Internuclear Distances Obtained by the Nonlinear Curve Fits of Cross-Relaxation Rates

Interproton vector	τ_{kl} (ns)	r_{kl} (Å)
G1H1′–H8	1.2	3.7
G1H5′–H3′	0.97	2.5
G1H1′–H2′	0.31	2.4
G1H1′–H2″	0.37	2.2
G1H5″–H3′	0.50	3.0
G1H3′–H2′	0.66	2.5
G1H8–C2H5	0.48	3.7
G1H2′–C2H6	0.49	2.7
G1H2″–C2H5	1.6	2.3
C2H6–H2′	2.4	2.2
C2H5′–H1′	0.89	3.1
C2H2″–H6	0.71	2.1
C2H1′–H6	0.40	3.3
C2H5–H2′	0.31	4.5
C2H3′–H2″	0.43	2.5
C2H1′–T3H6	0.25	4.8
C2H2′–T3H6	0.76	2.0
T3H3′–H2″	0.74	2.1
T3H4′–H3′	0.49	3.0
T3H1′–H6	0.45	4.0
T3H4′–H2″	0.48	3.1
G4H1′–H3′	0.16	3.0
T5H6–H3′	0.47	2.2
T5H1′–H6	0.87	3.5
T5H3′–H2′	0.57	2.5
T5H6–H2″	0.75	2.0
T5H2′–C6H6	0.64	2.6
T5H2″–C6H6	1.9	2.7
T5H2′–C6H5	0.88	2.6
C6H6–H3′	0.98	3.0
C6H1′–H2′	0.67	2.4
C6H6–H2′	0.63	2.5
C6H3′–G7H8	0.41	4.2
C6H2′–G7H5″	0.50	2.8
C6H2′–G7H8	0.89	2.8
C6H2″–G7H8	0.34	2.5
G7H5″–H3′	0.18	2.3
G7H5′–H3′	0.66	2.4
G7H1′–A8H8	0.52	2.9
A8H5′–H1′	2.6	3.1
A8H5′–H3′	0.54	2.7
A8H5″–H3′	0.22	2.4
A8H3′–H2″	0.50	2.8
A8H1′–A9H8	0.43	3.3
A8H2–A9H2	0.40	4.1
A9H1′–H2′	0.59	2.0
A9H1′–H8	0.94	3.3
A9H3′–H2″	1.8	2.7
A10H8–H3′	0.54	3.4
A10H8–H2″	0.67	2.3
A10H2″–G11H8	1.1	2.6
G11H1′–H8	0.57	2.6
G11H1′–C12H5″	0.58	2.8
G11H2″–C12H6	1.5	2.5
C12H6–H3′	0.49	2.9
C12H6–H1′	0.40	2.9
C12H5′–H6	0.45	2.6
C12H5–H2′	0.24	5.0

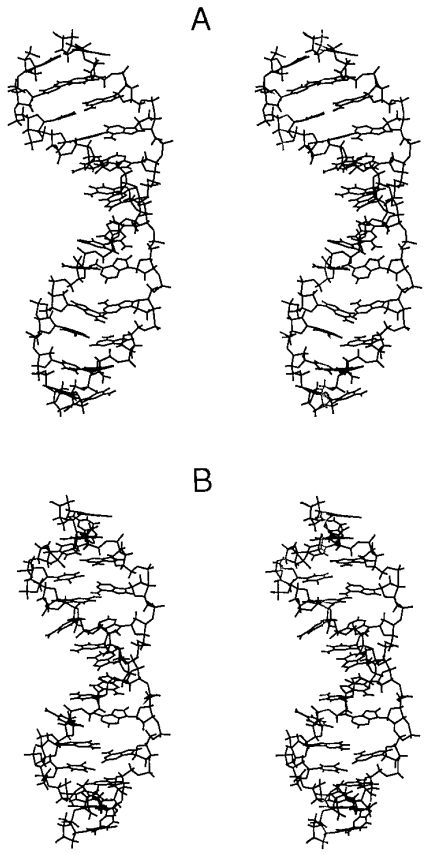

FIG. 7. Structure of a synthetic DNA duplex. (A) Average of 20 structures generated using NOESY, without including the variation of the rotational correlation time (τ_{kl}) for the calculation of internuclear distance (r_{kl}). (B) Average of 20 structures generated by the simulated annealing procedure described in the text, using the distance constraint set obtained by the complete relaxation matrix analysis of O-ROESY.

residue numbers in Fig. 8. *Sx* and *Sz* of mismatched (G4 and A9) and contiguous (T5 and A8) residues, and *Sy* of mismatched (G4 and A9) residues are significantly larger than those of other residues except for the terminal residues, and these tendencies are slightly more prominent in B conformation.

DISCUSSION

There are two ways to explain discrepancies between the ''experimentally'' obtained NOESY cross-peak intensities and those back-calculated from the ''optimized'' single structure derived from distance geometry or restrained molecular dynamics. One is an ensemble-averaged model where several structures are generated and averaged (*24*), and the other is the inclusion of the correct spectral densities for the rapid side chain or segmental fluctuations on the picosecond–nanosecond timescale and/or slower (~microsecond) conformational exchange motions. Such motions could be observed in the hydrophobic core region of proteins, for example, using O-ROESY (*25*), as described below. In the former approach, internal motions associated with exchange between multiple conformers are not included, while in the latter, the physical meaning of the ''average'' structure is somewhat uncertain; that is, it may include the average of different conformations with different internal motions.

Using O-ROESY data alone will be insufficient to fully characterize a molecule undergoing significant conformational fluctuations. However, here we will consider a simpler question. Can we experimentally separate the average internuclear distance from the spectral density function contribution to the average relaxation rate? Using a molecular dynamics simulation of antamanide, Brüschweiler *et al.* (*26*) suggested that the angular and the radial motion of internuclear vectors were almost separable. If we consider two spins under the dipole–dipole interaction in polar coordinates, the fluctuation of the radial part (internuclear distance) is orthogonal to those of angular variables. Therefore in a first approximation, it might be possible to average the internuclear distance and the spectral density function independently. This can provide a good starting point for consideration of structure and potentially conformational fluctuations.

Reduction of τ_{kl} in the intraresidue interproton vectors in G4 and intra- and interresidue vectors in G7, A8, A9 resulted in the relative reduction of r_{kl} values around these regions compared to other regions. Thus NOESY distance constraint set (a) with fixed τ_{kl} and O-ROESY distance constraint set (b) with inclusion of the variation of τ_{kl} yielded significantly different conformations. These calculations are based on the above assumption that the internuclear distance and the spectral density function are separable.

On the other hand, RMSD of 20 structures generated by constraint set (b) is slightly larger than that of (a), as shown in Table 2. One of the important causes of this may be the incomplete separability of τ_{kl} and r_{kl}. If motions of several internuclear vectors are strongly correlated, we may not be able to adequately separate τ_{kl} and r_{kl} of a nonbonded single

TABLE 2
Statistics of the Superimpositions of the Converged Structures

Restraints used for structure generation	a	b
RMSD (Å) of 20 structures	1.28 ± 0.32	1.43 ± 0.50
RMSD (Å) of average structure from the average structure A based on NOESY restraints		3.31
Relative potential energies of the final constrained energy minimized structures (kcal/mol)[a]	−608	−682

[a] Distance dependent dielectric constants were used, and no counter ions were included in the potential energy calculation.

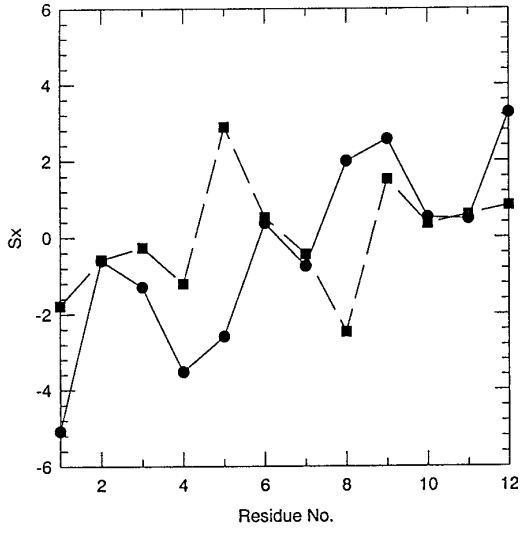

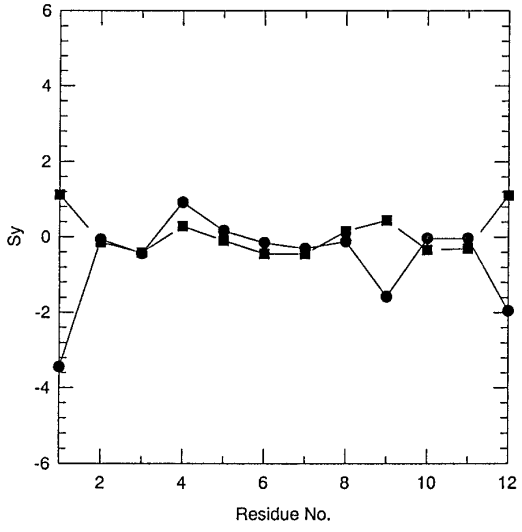

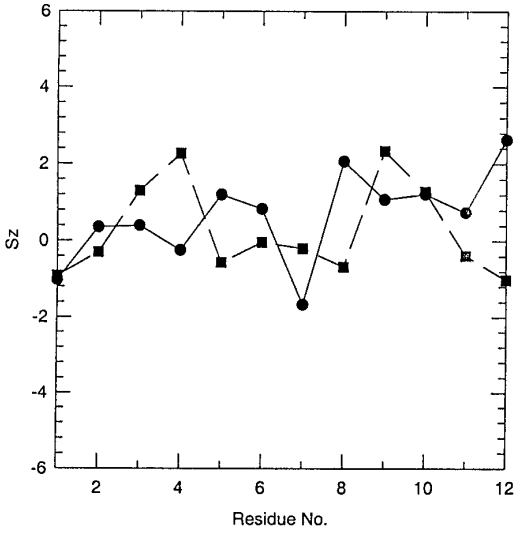

internuclear vector, resulting in less accuracy of the distance constraint. For example, we can plot τ_{kl} vs r_{kl} in Table 1 and easily find a clear relationship between two quantities, that is, τ_{kl} slightly decreases on increase of r_{kl}, for the interproton vectors between sugar and base. The relative internuclear motions between sugar and base may be somewhat statistically independent compared to those of intrasugar internuclear vectors. Therefore the internuclear correlations would decay earlier if they were spatially more apart. In this case, we may safely separate τ_{kl} and r_{kl}. In case of the intrasugar or the intrabase internuclear vectors, this relationship is unclear. However, to describe this particular tendency more accurately, more experimental data must be accumulated.

We conducted the nonrestrained molecular dynamics simulation of the same DNA double strand starting from the average structure B using AMBER potential field (*18*). Although the auto-correlation functions of the internuclear vectors between H1′ and H8(6) were rather complex, those of mismatched and contiguous residues decayed earlier compared to others (data not shown). Although the correlation time derived here is simply a correlation time, it may be possible to utilize a more sophisticated spectral density function, such as Lipari–Szabo type, and examine other internal motion models by nonlinear square fitting of a few curves emanating from protons on a selected part of the molecule. It might also be possible to characterize complex motions of nuclei in biological macromolecules by a network-like combination of multiple internuclear vectors with spectral density functions of Lorentzian type.

O-ROESY cross-relaxation rate dispersion curve as a function of ν_{irrad} can yield τ_{kl} and r_{kl} using the complete relaxation matrix approach. This also eliminates difficulties mentioned in the author's previous papers (*3, 6*) and provides a new method for obtaining dynamical information and structural restraints. An advantage of O-ROESY complete relaxation matrix analysis is that using a static magnetic field, we can determine τ_{kl} without any assumption of r_{kl} nor three-dimensional structure. In the case of G–A mismatches, specific cleavage by the repair enzyme Mut Y entails recognition of the structural features at the mismatched site (*27–30*). Knowledge of the rotational correlation time is essential to obtain accurate distance constraints and subsequently accurate three-dimensional structure. The 1D soft off-resonance ROESY method (*31*) applied to β-cyclodextrin is certainly appropriate for the small-sized molecule, whereas the O-ROESY method combined with complete relaxation ma-

FIG. 8. Global interbase pair parameters, shear (*Sx* Å), stretch (*Sy* Å), and stagger (*Sz* Å), vs residue number are plotted for structure A (●) and B (■). Parameters were calculated using Curve 4.1 (*19*). *Sx* and *Sz* of mismatched (G4 and A9) and contiguous (T5 and A8) residues, and *Sy* of mismatched (G4 and A9) residues are significantly larger than those of other residues except for the terminal residues (see text).

trix analysis is suitable for complex biological macromolecules undergoing significant spin-diffusion.

If there is slow exchange process of the ~millisecond timescale, the cross-peak intensity of O-ROESY spectra should be reduced. However, in general, the contribution of chemical shift fluctuation on the relaxation rate is expected to be rather small in ^{1}H spectra at room temperature. Therefore, we just incorporated an exchange matrix according to the ordinal MARDIGRAS procedure (*32*).

On the other hand, $T_{1\rho}^{\text{off}}$ values obtained from 1D spectra of bovine pancreatic trypsin inhibitor (BPTI) under 10–100 kHz off-resonance irradiation field showed no significant change. However, O-ROESY cross-peak intensities of the internal hydrophobic core residues exhibited slight oscillation as a function of ν_{irrad}, while those of surface residues showed smooth dispersive behaviors. Slow exchange motion of ~millisecond timescale could be observed for a solid-like core region in protein interior using O-ROESY (*25*). If an internuclear vector undergoes dominantly ~millisecond intramolecular motion with less ~nanosecond intramolecular motion, there would be an interference between the exchange superoperator (~millisecond timescale) and the spin Hamiltonian in the rotating fame (~kilohertz frequency) under the off-resonance irradiation field, resulting in the accumulation of geometrical phase (*33*), which should be a function of ν_{irrad}.

In a recent publication (*6*), we made several corrections for the original O-ROESY analysis (*3*); i.e., we cannot neglect the contribution of internuclear distance (r_{kl}) for the analysis of the normalized cross-peak intensity dispersion curve as a function of ν_{irrad} when r_{kl} is shorter (*6*). In general, cross-peak intensity is a function of multiple parameters, including external relaxation (*3*), spectral density function, and r_{kl}. This multiple-parameter dependency of the cross-peak intensity can be essentially removed by the complete relaxation matrix analysis presented here. By a nonlinear curve fit of the cross relaxation rates as a function of ν_{irrad}, we can obtain the order parameter (S) and the effective correlation time (τ_e) in the Lipari–Szabo spectral density function (*7*) for all the observed internuclear vectors relative to reference parameters, S_0 and τ_{e0}, respectively, as described in Appendix II. If we could use two kind of different static magnetic fields, we could obtain S and τ_e uniquely without any reference internuclear vector using simulated relaxation rates (data not shown).

CONCLUSION

Refinement of distance constraints using the O-ROESY technique significantly affected the final three-dimensional DNA structure obtained using the restrained molecular dynamics. Heterogeneous internal motions significantly contribute to the cross-peak intensities of O-ROESY spectra. This report demonstrated that the terminal, mismatched, and contiguous regions of a DNA duplex had relatively large flexibility compared to other regions. The average structure obtained by restrained molecular dynamics simulation with inclusion of variations of the rotational correlation times also indicated a tendency of the mismatched and contiguous bases to flip to the outside of the double strand.

In conclusion, the complete relaxation matrix analysis method for O-ROESY offers an advantage for the refinement of distance constraints and investigation of internal molecular dynamics. No isotope labeling nor static magnetic field dispersion is required for the estimation of the specific internal molecular motion. It is potentially possible to examine the internal motions of the interproton vectors corresponding to long distance interproton NOEs, which may be quite important in understanding biological macromolecular function.

APPENDIX I

Let us consider two spins, k and l, interacting via J coupling. We assume a single irradiation by a radiofrequency (RF) wave of angular frequency ω_{RF}, with field strength B_2. The inner product of spin operators in the scalar coupling Hamiltonian, $\mathbf{I}_k \cdot \mathbf{I}_l = I_{kz}I_{lz} + \frac{1}{2}(I_{k+}I_{l-} + I_{k-}I_{l+})$ is transformed into the doubly rotating frame (*4*) as

$$\begin{aligned}(c_kc_l + s_ks_l)I'_{kz}I'_{lz} + \tfrac{1}{2}(c_ks_l - s_kc_l)(e^{-i\Omega_l t}I'_{kz}I'^{+}_{l} + e^{i\Omega_l t}I'_{kz}I'_{l-}) \\ + \tfrac{1}{2}(s_kc_l - c_ks_l)(e^{-i\Omega_k t}I'_{k+}I'_{lz} + e^{i\Omega_k t}I'_{k-}I'_{lz}) + \tfrac{1}{4}(s_ks_l \\ + c_kc_l + 1)(e^{-i(\Omega_k+\Omega_l)t}I'_{k+}I'_{l+} + e^{i(\Omega_k+\Omega_l)t}I'_{k-}I'_{l-}) \\ + \tfrac{1}{4}(s_ks_l + c_kc_l + 1)(e^{-i\Delta t}I'_{k+}I'_{l-} + e^{i\Delta t}I'_{k-}I'_{l+}) \qquad [4]\end{aligned}$$

in which $\Delta = \Omega_k - \Omega_l$; $\Omega_i = \{(\omega_i - \omega_{\text{RF}})^2 + \omega_2^2\}^{1/2}$; ω_i is the Larmor precession frequency of spin i ($i = k, l$); ω_2 is γB_2; s_i and c_i ($i = k, l$) indicate sin β_i and cos β_i, respectively; and β_i is the tilt angle of the quantization axis of spin i from the z axis. In the superimposed tilted doubly rotating frame (STDRF) (*11*), spin k precesses with a frequency Δ relative to spin l around the quantization axis. The last terms corresponding to the ZQT (including Δ) in Eq. [4] survive in STDRF under the condition $\Omega_k, \Omega_l \gg J$. Finally, the effective scalar interaction in STDRF is obtained as

$$\Omega_{\text{R}} = \frac{J}{2}(1 + \cos(\beta_k - \beta_l)), \qquad [5]$$

where Ω_{R} can be also interpreted as a generalized Rabi frequency.

For the dressed state calculation of the ZQT probability, we must prepare a projection operator (*12*) $P = |\varphi_k\rangle\langle\varphi_k| + |\varphi_l\rangle\langle\varphi_l|$, and its supplementary operator $Q = 1 - |\varphi_k\rangle\langle\varphi_k|$

$- |\varphi_l\rangle\langle\varphi_l|$. Also $G(z)$ and $R(z)$ are defined as the resolvent of the Hamiltonian and the level-shift operator, respectively, where z is a complex variable. Projection of $G(z)$ in $\mathbf{E}_0$, which is a subspace of the space of states subtended by an ensemble of eigenvectors of $H_0\{|\varphi_k\rangle, |\varphi_l\rangle\}$, can be calculated as

$$PG(z)P = \begin{bmatrix} G_{kk}(z) & G_{kl}(z) \\ G_{lk}(z) & G_{ll}(z) \end{bmatrix}$$

$$= \begin{bmatrix} z - E_k - R_{kk}(z) & -R_{kl}(z) \\ -R_{lk}(z) & z - E_l - R_{ll}(z) \end{bmatrix}^{-1} \quad [6]$$

$$= \frac{1}{(z - E_k - R_{kk}(z))(z - E_l - R_{ll}(z)) - R_{kl}R_{lk}} \times \begin{bmatrix} z - E_l - R_{ll}(z) & -R_{lk}(z) \\ -R_{kl}(z) & z - E_k - R_{kk}(z) \end{bmatrix}. \quad [7]$$

The off-diagonal matrix element is

$$G_{kl}(z) = \frac{V_{lk}}{(z - E_k)(z - E_l) - |V_{kl}|^2}, \quad [8]$$

where $V_{kl} = V_{lk} = h\Omega_R/4\pi$. Here, we switch to STDRF which gives a convenient quantum number and define new energy levels, $E_1 = (E_k + E_l)/2 + h\Omega_R/4\pi$ and $E_2 = (E_k + E_l)/2 - h\Omega_R/4\pi$. The transition amplitude U_{kl}, for $t > 0$, is

$$U_{kl} = \frac{1}{2\pi i}\int_{C+} dz \exp\left(-\frac{2\pi i z t}{h}\right) G_{kl}(z)$$

$$= V_{kl}\left[\frac{1}{E_1 - E_2}\exp\left(-\frac{2\pi i E_1 t}{h}\right) + \frac{1}{E_2 - E_1}\exp\left(-\frac{2\pi i E_2 t}{h}\right)\right]$$

$$= -\frac{i\Omega_R}{\Omega}\exp\left[-\frac{\pi i(E_1 + E_2)t}{h}\right]\sin\frac{\Omega t}{2}, \quad [9]$$

where $\Omega^2 = \Delta^2 + \Omega_R^2$, and C_+ indicates that the integration covers the contour from right to left along the real axis in the upper half of the complex plane (*12*). When we vary the phase and/or amplitude of the small pulses within a shaped pulse, we can calculate the final transition probability using Eq. [9]. This is one of the novel aspects of the proposed theory. In case of the shaped pulse of constant phase increment and constant amplitude, we finally obtain the well-known transition probability $P_{kl}(t)$:

$$P_{kl}(t) = |U_{kl}(t)|^2 = \frac{\Omega_R^2}{\Omega^2}\sin^2\left(\frac{\Omega t}{2}\right). \quad [10]$$

Energy levels E_1 and E_2 manifest the anticrossing (*12*) at the Hartman–Hahn match condition (*11*) with the minimum energy difference, $h\Omega_R/2\pi$.

APPENDIX II

We can determine relatively two variables of the spectral density function for each internuclear vector using a series of O-ROESY experiment. For simplicity, here we use the spectral density function of Lipari–Szabo (*7*). It may be possible to determine both S and τ_e relative to the reference values by fitting the cross-relaxation rates $\sigma_{\text{O-ROE}}$ derived from the complete relaxation matrix analysis for O-ROESY. If σ_{NOE} and $\sigma_{ROE(-)}$, which is σ_{ROE} without J-coupled ZQT contribution, can be determined independently, S and τ_e can be also determined uniquely. However, to obtain τ_0, which is common for all the intramolecular internuclear vectors, we must conduct another independent experiment, such as a ^{13}C off-resonance rotating-frame spin–lattice relaxation experiment (*34*).

To determine σ_{NOE} and $\sigma_{ROE(-)}$ independently, we need to have the reference internuclear vector with known σ_{NOE_0}, σ_{ROE_0} (which does not include J-coupled ZQT contribution), and internuclear distance, r_0. If a cross-relaxation rate is normalized to this reference, we can obtain a ratio

$$\sigma_i = \frac{r^6(a_i\sigma_{NOE} + b_i\sigma_{ROE})}{r_0^6(c_i\sigma_{NOE_0} + d_i\sigma_{ROE_0})}, \quad [11]$$

where $a_i \sim d_i$ are the trigonometric coefficients which are functions of the chemical shifts of the spins and off-resonance spin-lock frequency. If we know the exact two $\sigma_{\text{O-ROE}}$ values, i.e., σ_1 and σ_2 at two different off-resonance frequencies, we can determine σ_{NOE} and $\sigma_{ROE(-)}$ as

$$\sigma_{NOE} = \frac{1}{a_1b_2 - a_2b_1}\frac{r_0^6}{r^6}\{\sigma_1b_2(c_1\sigma_{NOE_0} + d_1\sigma_{ROE_0}) - \sigma_2b_1(c_2\sigma_{NOE_0} + d_2\sigma_{ROE_0})\} \quad [12]$$

$$\sigma_{ROE(-)} = \frac{1}{a_2b_1 - a_1b_2}\frac{r_0^6}{r^6}\{\sigma_1a_2(c_1\sigma_{NOE_0} + d_1\sigma_{ROE_0}) - \sigma_2a_1(c_2\sigma_{NOE_0} + d_2\sigma_{ROE_0})\}. \quad [13]$$

By a nonlinear curve fit of the cross relaxation rates as a function of off-resonance frequency, we can get S and τ_e

for all the observed internuclear vectors relative to S_0 and τ_{e0}, respectively.

ACKNOWLEDGMENTS

We thank Mr. James Loo at UCSC for technical support in 3D O-ROESY measurements and Dr. Sheila David and Mr. Bruce Meads for preparation of the DNA oligonucleotide sample in these studies. We thank Dr. Herve Desvaux at CIMAR/NHMFL and Dr. Nicolas Birlirakis at ICSN-CNRS in France for helpful discussion at 37th ENC. We thank Dr. Seiichi Era for general helpful support. The research was supported by Special Grants-in-Aid 07280207 from the Ministry of Education, Science and Culture of Japan as well as the KOKUSAI HIYAKU (in Japanese) award of Japan Society of Magnetic Resonance in Medicine, National Institutes of Health Grants EY04033 and GM39247.

REFERENCES

1. B. A. Borgias and T. L. James, *J. Magn. Reson.* **87,** 475 (1990).
2. T. L. James and V. J. Basus, *Annu. Rev. Phys. Chem.* **42,** 501 (1991).
3. K. Kuwata and T. Schleich, *J. Magn. Reson. A* **111,** 43 (1994).
4. K. Kuwata and T. Schleich, *J. Magn. Reson. A* **114,** 219 (1995).
5. H. Desvaux, P. Berthault, N. Birlirakis, and M. Goldman, *J. Magn. Reson. A* **108,** 219 (1994).
6. D. Brooks, L. Patrick, K. Kuwata, and T. Schleich, *J. Magn. Reson. A* **117,** 307 (1995).
7. G. Lipari and A. J. Szabo, *J. Am. Chem. Soc.* **104,** 4546 (1982).
8. S. L. Patt, *J. Magn. Reson.* **95,** 94 (1991).
9. G. Otting, E. Liepinsh, and K. Wüthrich, *Science* **254,** 974 (1991).
10. R. Bazzo, C. J. Edge, M. R. Wormald, T. W. Rademacher, and R. A. Dwek, *Chem. Phys. Lett.* **174,** 313 (1990).
11. G. C. Chingas, R. D. Garroway, R. D. Bertrand, and W. B. Moniz, *J. Chem. Phys.* **74,** 127 (1981).
12. C. Cohen-Tannoudji, J. Dupont-Roc, and G. Grynberg, ''Atom-Photon Interactions,'' Wiley, New York, 1992.
13. M. M. Maricq, *Adv. Magn. Reson.* **14,** 151 (1990).
14. H. Widmer and K. Wüthrich, *J. Magn. Reson.* **70,** 270 (1986).
15. H. Widmer and K. Wüthrich, *J. Magn. Reson.* **74,** 331 (1987).
16. E. Nikonowicz and D. G. Gorenstein, *Biochemistry* **29,** 8845 (1990).
17. C. Gonzalez, W. Stec, A. Kobylanska, R. I. Hogrefe, M. Reynolds, and T. L. James, *Biochemistry* **33,** 11062 (1994).
18. P. K. Weiner, P. A. Kollman, D. T. Nguyen, and D. Case, *J. Comput. Chem.* **7,** 230 (1986).
19. R. Lavery and H. J. Sklenář, *Biomol. Struct. Dynam.* **6,** 63 (1988).
20. J. Feigon, W. Leupin, W. A. Denny, and D. R. Kearns, *Biochemistry* **22,** 5943 (1984).
21. R. M. Scheek, R. Boelens, N. Russo, J. H. van Boom, and R. Kaptein, *Biochemistry* **23,** 1371 (1984).
22. R. Boelens, R. M. Scheek, K. Dijkstra, and R. Kaptein, *J. Magn. Reson.* **62,** 371 (1985).
23. K. Kuwata and T. Schleich, *J. Magn. Reson. B* **104,** 11 (1994).
24. U. Schmitz, A. Kumar, and T. L. James, *J. Am. Chem. Soc.* **114,** 10654 (1992).
25. K. Kuwata and S. Era, 11th Rinshoken International Conference, Abstract 73 (1996).
26. R. Brüschweiler, B. Roux, M. Blackledge, C. Griesinger, M. Karplus, and R. R. Ernst, *J. Am. Chem. Soc.* **114,** 2289 (1992).
27. B. Kramar, W. Kramar, and H. J. Fritz, *Cell* **38,** 879 (1984).
28. K. G. Au, S. Clark, J. H. Miller, and P. Modrich, *Proc. Natl. Acad. Sci.* **86,** 8877 (1989).
29. S. Klimasauskas, S. Kumar, R. J. Roberts, and X. Cheng, *Cell* **76,** 357 (1994).
30. D. G. Vassylyev, T. Kashiwagi, Y. Mikami, M. Ariyoshi, S. Iwai, E. Ohtsuka, and K. Morikawa, *Cell* **83,** 773 (1995).
31. H. Desvaux, P. Berthault, and N. Birlirakis, *Chem. Phys. Lett.* **233,** 545 (1995).
32. H. Liu, A. Kumar, K. Weisz, U. Schmitz, K. D. Bishop, and T. L. James, *J. Am. Chem. Soc.* **115,** 1590 (1993).
33. D. Suter, G. C. Chingas, R. A. Harris, and A. Pines, *Mol. Phys.* **61,** 1327 (1987).
34. T. Schleich, C. F. Morgan, and G. H. Caines, *Methods Enzymol.* **176,** 386 (1989).